Clays and Clay Minerals, Vol. 47, No. 4, 425–438, 1999.

AMBIENT-TEMPERATURE SYNTHESIS, EVOLUTION, AND CHARACTERIZATION OF COBALT-ALUMINUM HYDROTALCITE-LIKE SOLIDS

HILLARY A. THOMPSON,[1,†] GEORGE A. PARKS,[1] AND GORDON E. BROWN, JR.[1,2]

[1] Department of Geological and Environmental Sciences, Stanford University, Stanford, California 94305-2115, USA
[2] Stanford Synchrotron Radiation Laboratory, Stanford, California 94309, USA

Abstract—Double hydroxide solids precipitated homogeneously from three laboratory-synthesized aqueous solutions that simulated mildly contaminated surface or groundwater. Over a limited pH range, precipitates formed rapidly from dissolved ions, and more slowly by incorporating ions dissolving from other solids, including highly soluble aluminous solids. The precipitates were characterized by size and shape via transmission electron microscopy (TEM), by composition via inductively coupled plasma-mass spectrometry (ICP-MS) of mother solutions and analytical electron microscopy (AEM) of precipitates, and by structure via powder X-ray diffraction (XRD), TEM, and extended X-ray absorption fine structure (EXAFS) spectroscopy. They were identified as nanocrystalline cobalt hydrotalcite (CoHT) of the form $[Co(II)_{1-x}Al(III)_x(OH)_2]^{x+}(A^{n-}_{x/n})\cdot mH_2O$, with x = 0.17–0.25, A = CO_3^{2-}, NO_3^-, or $H_3SiO_4^-$, n = anion charge and m undetermined. Complete solid solution may exist at the macroscopic level for the range of stoichiometries reported, but clustering of Co atoms within hydroxide layers indicates a degree of immiscibility at the molecular scale. Composition evolved toward the Co-rich endmember with time for at least one precipitate. The small layer charge in the x = 0.17 precipitate caused anionic interlayers to be incomplete, producing interstratification of hydrotalcite and brucite-like layers. Solubility products estimated from solution measurements for the observed final CoHT stoichiometries suggest that CoHT is less soluble than the inactive forms of $Co(OH)_2$ and $CoCO_3$ near neutral pH. Low solubility and rapid formation suggest that CoHT solids may be important sinks for Co in contact with near neutral pH waters. Because hydrotalcite can incorporate a range of transition metals, precipitation of hydrotalcite may be similarly effective for removing other trace metals from natural waters.

Key Words—Anionic Clay, Cation Ordering, Coprecipitation, EXAFS, Hydrotalcite, ICP-MS, Solubility Product, TEM, Metal Contamination, Solid Solution, Interstratification.

INTRODUCTION

The partitioning of toxic metal ions between solid and solution phases controls metal-ion mobility in the environment. Metal-ion mobility is limited by chemical interactions that adhere metal ions to the surfaces of host minerals. In addition, homogeneous precipitation of metal ions potentially renders them less mobile, if the resulting particles are sufficiently large to resist movement or if they adhere to other host minerals as a surface precipitate. Researchers modeling metal-ion mobility traditionally consider, at most, precipitation of stoichiometric single metal hydroxides and adsorption on existing solid surfaces as routes for solid phase partitioning (Schindler *et al.*, 1987). Solid-solution formation is seldom considered in low temperature calculations, with notable exceptions (Farley *et al.*, 1985; Bruno *et al.*, 1998).

Several laboratory studies of metal ion partitioning identify the precipitation of mixed metal hydroxides known as hydrotalcites as a significant uptake route for metal ions (d'Espinose de la Caillerie *et al.*, 1995; Scheidegger *et al.*, 1997; Towle *et al.*, 1997; Thompson *et al.*, 1999). Although precipitation was shown to be homogeneous in one highly concentrated system (d'Espinose de la Caillerie *et al.*, 1995), it is not known whether hydrotalcites form homogeneously under less concentrated conditions, because they were only detected in association with the bulk solid phase following partial phase separation. The nanoscale size of some hydrotalcites (Yun and Pinnavaia, 1995; Scheidegger *et al.*, 1996; Thompson, 1998) makes the homogeneous *vs.* heterogeneous distinction important for metal-ion transport. Furthermore, it is currently not possible to consider hydrotalcite precipitation in geochemical modeling of laboratory experiments and field environments, because thermodynamic data have not been determined for hydrotalcites, with few exceptions (Crovisier *et al.*, 1986; Bennett *et al.*, 1992; Boclair and Braterman, 1999; Boclair *et al.*, 1999).

Hydrotalcite-like compounds are composed of positively-charged, trioctahedral hydroxide layers alternating with layers of hydrated anions (Figure 1). Divalent and trivalent metal cations (M(II) and M(III)) occupy the same crystallographic site in the hydroxide layers, resulting in $[M(II)_{1-x}M(III)_x(OH)_2]^{x+}(A^{n-}_{x/n})\cdot mH_2O$, with x = 0.17–0.33, n typically 1 or 2, and m highly variable. Hydrotalcites contain a variety of cations, including Mn(II), Fe(II), Co(II), Ni(II), Cu(II), Zn(II), Al(III), Cr(III), Mn(III), Fe(III), Co(III) (Feit-

† Present address: Los Alamos National Laboratory, MS D469, Los Alamos, New Mexico 87545, USA.

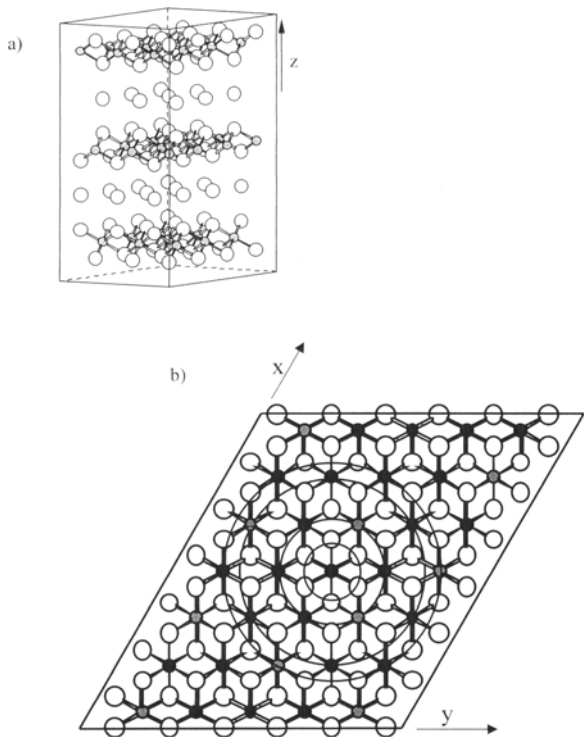

Figure 1. Structure of hydrotalcite. a) View parallel to (001) showing hydroxide layers (top, middle, and bottom) interlayered with O atoms from hydration water. Each hydroxide layer contains divalent and trivalent metal cations in a 3:1 ratio, respectively. Anions and water hydrogens not shown. b) Two-dimensional representation of a single hydroxide layer, view perpendicular to (001). Assuming a cobalt hydrotalcite composition, Co in black, Al in grey, O in white. Atoms are grouped by distance from the central Co atom using concentric circles, much as neighboring atom information is grouped by distance in the Fourier transform of a Co EXAFS spectrum. With increasing radius, circles join nearest neighbor O atoms (2.1 Å), second neighbor Co1 and Al1 (3.1 Å), more distant Co2 and Al2 (5.3 Å), and most distant (of atoms included in EXAFS data fits) Co3 and Al3 (6.2 Å).

knecht, 1942; Allmann, 1970; Cavani *et al.*, 1991). Anions including CO_3^{2-}, SO_4^{2-}, NO_3^-, OH^-, Cl^- and Br^- occupy the interlayer (Miyata, 1983). The relative abundance of some of these moieties at the earth's surface (Mn, Fe, Al, CO_3^{2-}, and OH^-) and concern about the environmental impact of others (Co, Ni, Cu, Cr, SO_4^{2-}, NO_3^-, CO_3^{2-}) suggest that precipitation of hydrotalcites may be an important set of reactions for environmental geochemistry. For compositions including redox-active elements, hydrotalcites are also important for their ability to participate in electron-transfer processes that limit metal-ion mobility, as seen for the reduction of Se(VI) to its less mobile, zero-valent state by the ferrous-ferric hydrotalcite known as green rust (Myneni *et al.*, 1997).

Hydrotalcites are employed as industrial catalysts and catalyst supports for oxidation and condensation reactions (Reichle, 1985), soil remediation (Yun and Pinnavaia, 1995), anion exchange, and medication (Cavani *et al.*, 1991), and therefore have been characterized in the catalysis literature. Catalytic hydrotalcites are synthesized under extreme conditions relative to nature, *e.g.*, high concentrations of constituent ions (0.1 M), high pH (8–11), and high temperature calcination (60–1000°C), and therefore may not be similar to those that would form in nature. Synthesis of hydrotalcites under less extreme conditions was addressed infrequently since Feitknecht (1942).

This study was conducted to determine if hydrotalcite-like phases could precipitate homogeneously from dilute aqueous solutions of Co and Al at ambient temperature and, if so, to characterize the size, structure, composition, and stability of precipitated products. Three precipitates were synthesized from aqueous solutions that differed in ion concentration and pH and were undersaturated with respect to the stable form of $Co(OH)_2$. Solution composition was varied to examine its effect on product composition and the formation of impurity phases. Precipitated products were characterized by powder X-ray diffraction (XRD), extended X-ray absorption fine structure (EXAFS) spectroscopy, transmission electron microscopy (TEM), and analytical electron microscopy (AEM); dissolved ion concentrations were measured by inductively coupled plasma-mass spectrometry (ICP-MS). Solubility products were estimated from solution data.

MATERIALS AND METHODS

Synthesis

Three precipitates (CoHT-1, CoHT-2, and CoHT-4) were synthesized in air or N_2 boil-off environments from solutions that differed in initial ion concentration, pH, and sequence of ion mixing and pH adjustment, as outlined below and summarized in Table 1. Experiments were conducted at ambient temperature (20–23°C). Solution pH was measured with an Orion Ross Combination electrode calibrated before each use and every two hours during extended use. Experiments extended for hundreds to thousands of hours, and reaction vessels generally remained sealed to minimize evaporation. For experiments conducted in air, sealed vessels also limited equilibration with atmospheric CO_2, as discussed below. Water was treated by a MilliQ ion-exchange system. Experiments used polycarbonate or polypropylene labware and Teflon magnetic stir bars. Reagents never contacted glass labware (other than the electrode), with the exception of an autotitrator with glass burets used during the first 16 h of the CoHT-2 experiment. The onset of precipitation was detected by scattering of HeNe laser light passing through the solution.

COHT-1. This experiment followed the procedure outlined by Taylor (1984) for his experiment #25334 to

https://doi.org/10.1346/CCMN.1999.0470405 Published online by Cambridge University Press

Table 1. Summary of initial and subsequent experimental conditions. Ion concentrations are based on total experiment volume, *i.e.*, after mixing separate reagent solutions.

Experiment	Age[1] [h]	Env[2]	pH[3]	Co[4] [mM]	Al[4] [μM]	Co:Al	Si[4] [μM]	Na[5] [M]	CO_3 added[6] [M]	Eqm. CO_3[7] [mM]	NO_3[8] [M]
CoHT-1	0	Air	6.90	45.0	12,000	3.75	0	0.039	0.0196	—	0.128
CoHT-1	1063	Air	7.09	6.80	0.04		4.0	0.112	0.0553	0.109	0.142
CoHT-1	2765	Air	7.12	6.86	0.07		4.1	0.112	0.0553	0.117	0.142
CoHT-2	0	Air	7.82	1.35	38	36	0[9]	0.113	0	—	0.116
CoHT-2	983	Air	7.78	1.31	0.03		19[9]	0.113	0	0.406	0.116
CoHT-2	2687	Air	7.82	1.29	0.05		20[9]	0.113	0	0.445	0.116
CoHT-4	0	N_2	7.82	1.45	63	23	130	0.111	0	—	0.11
CoHT-4	0.4	N_2	7.73	1.20	0.02		78	0.111	0	excluded	0.11
CoHT-4	33	N_2	7.71	1.18	0.02		48	0.111	0	excluded	0.11

[1] Sample age is defined relative to the time the target pH was first achieved in a solution containing Co and Al.
[2] Synthesis environment.
[3] Measured pH.
[4] Co, Al, and Si concentrations were measured by ICP-MS.
[5] Na, CO_3, and NO_3 concentrations were calculated, and therefore reflect changes with time owing to titrant additions. Na was calculated from Na_2CO_3 titrant additions (CoHT-1), and from $NaNO_3$ electrolyte and NaOH titrant additions (CoHT-2 and CoHT-4).
[6] "CO_3 added" was calculated from Na_2CO_3 additions (CoHT-1).
[7] "Eqm. CO_3" was calculated using Hydraql (Papelis *et al.*, 1988) assuming equilibrium with atmospheric carbon dioxide (CoHT-1 and CoHT-2), which required net release of dissolved carbonate from CoHT-1 and net addition of dissolved carbonate to CoHT-2, relative to carbonate added at the outset of experiments.
[8] NO_3 was calculated from $Al(NO_3)_3$, $Co(NO_3)_2$, and HNO_3 additions (CoHT-1) and additionally $NaNO_3$ but not HNO_3 (CoHT-2 and CoHT-4).
[9] CoHT-2 silicate was added unintentionally by dissolution of glass burets containing acid and base titrant.

permit comparison with the Ni hydrotalcite he synthesized and characterized. In air, separate 100-mL aqueous solutions of 24 mM $Al(NO_3)_3$ and 90 mM $Co(NO_3)_2$ were titrated to pH 6.9 with ≤1 M Na_2CO_3. Laser light scattering was apparent in each solution at pH 6.9. The solutions were mixed and pH drifted to lower values for 3–5 h, then to higher values for the remainder of the experiment. Depending on the direction of pH drift, dilute HNO_3 or Na_2CO_3 was added periodically to restore pH to 6.9, with maximum drift of +0.2 to −0.3 pH units. The reaction vessel remained open to air for the first 30 h, after which it was sealed and opened only for sampling and pH measurement.

COHT-2 and COHT-4. These experiments simulated the solution conditions of sorption experiments reported in Thompson (1999) to allow a comparison between homogeneous precipitates and those that form in the presence of minerals. Accordingly, initial Al and Si concentrations approximated those present in the uptake experiments through dissolution of kaolinite, the sorption substrate. Initial Co concentration and pH adjustment history were also adopted from uptake experiments. Cobalt concentrations were considerably more dilute than in the CoHT-1 experiment, and mixing preceded the pH increase. The CoHT-2 experiment was conducted in air, and the CoHT-4 experiment was conducted in a N_2-purged glove box.

In the CoHT-2 experiment, 50-mL solutions of 2.7 mM $Co(NO_3)_2$ and 75 μM $Al(NO_3)_3$, each in 0.1 M $NaNO_3$ with pH pre-adjusted to 4.5, were filtered through a 0.2 μm Nylon syringe filter into a 100-mL polypropylene bottle. Laser light was not scattered by the mixed solution at pH 4.5. For the next 45 min, the solution was titrated with 0.1 M NaOH to pH 7.8, where it was held within ±0.02 pH units. Laser light scattering was apparent by pH 7.0.

In the CoHT-4 experiment, sufficient acidic $Al(NO_3)_3$, aqueous Si, and 0.1 M $NaNO_3$ at pH 4.5, were added to a 100-mL polypropylene volumetric flask to achieve a final solution containing 126 μM Al and 266 μM Si in 0.1 M $NaNO_3$. This solution was passed through an 0.2-μm Nylon syringe filter into a 250-mL polycarbonate bottle. The pH of the mixed Al and Si solution was 3.16. After filtering, 100 mL of 2.9 mM aqueous $Co(NO_3)_2$ in 0.1 M $NaNO_3$, with pH pre-adjusted to 4.5, was added to the same bottle. The pH for the mixed Al, Si, and Co solution was 3.45, and the solution did not scatter a laser beam. The solution was titrated with 0.1 M NaOH to pH 7.82 over a 1.3 h period. Scattering of the laser beam began at pH = 5.3. Once achieved, pH was maintained within +0.09 to −0.16 pH units of 7.82 for 674 h (28 d), after which the entire slurry was filtered on a 0.1-μm polycarbonate filter membrane.

Analysis

Samples were collected periodically from each well-mixed experiment. Filtered (0.2 μm Nylon) supernatants were analyzed for dissolved Co, Al, and Si by

https://doi.org/10.1346/CCMN.1999.0470405 Published online by Cambridge University Press

Table 2. Logarithms of equilibrium constants (tabulated as $-\log K_{sp}$) for *formation* of aqueous and solid species. Formation reactions (except for Co-Al-silicate solids, see footnote 8) are constructed from H_2O and basic components as defined in the program HYDRAQL (Papelis *et al.*, 1988), which include Al^{3+}, $H_2SiO_4^{2-}$, Co^{2+}, H^+, NO_3^-, CO_3^{2-}, *e.g.*, $Co^{2+} + 3\ H_2O \leftrightarrow Co(OH)_3^{1-} + 3\ H^+$; $-\log K_{sp}$, $Co(OH)_3^{1-} = \log\{Co(OH)_3^{1-}\} + 3\ \log\{H^+\} - \log\{Co^{2+}\} = -31.5$, where { } indicates activity.

Aqueous species		Solids	
Al^{3+}		Aluminum	
$Al(OH)^{2+}$	−5.00[1]	Gibbsite, $Al(OH)_3$	−8.12[5]
$Al(OH)_2^+$	−10.10[1]	Amorphous $Al(OH)_3$	−9.66[5]
$Al(OH)_3^0$	−16.80[1]	Boehmite, AlOOH	−8.00[5]
$Al(OH)_4^-$	−22.99[1]	Bayerite, $Al(OH)_3$	−9.15[5]
$H_2SiO_4^{2-}$		Aluminosilicate	
$H_3SiO_4^-$	13.09[2]	Kaolinite, $Al_2Si_2O_5(OH)_4$	40.13[5]
$H_4SiO_4^0$	22.92[2]	Halloysite, $Al_2Si_2O_5(OH)_4$	36.76[5]
Co^{2+}		Imogolite, $HOSiO_3Al_2(OH)_3$	10.74[5]
$CoCO_3^0$	4.41[3]	Pyrophyllite, $Al_2Si_4O_{10}(OH)_2$	92.76[5]
$CoHCO_3^+$	12.5[3]		
$Co(CO_3)_2^{2-}$	7.46[3]		
$CoNO_3^+$	0.20[4]		
$Co(NO_3)_2^0$	0.66[4]		
$CoOH^+$	−9.65[2]	Silica	
$Co(OH)_2^0$	−18.8[2]	Quartz, SiO_2	26.92[2,6]
$Co(OH)_3^{1-}$	−31.5[2]	Amorphous SiO_2	25.66[2,6]
$Co(OH)_4^{2-}$	−46.3[2]	Cobalt	
Co_2OH^{3+}	−11.20[2]	$CoCO_3$	10.12[7]
$Co_4(OH)_4^{4+}$	−30.53[2]	$Co(OH)_2$ pink	−12.28[2]
		$Co(OH)_2$ blue	−13.78[2]
		Cobalt-Aluminum	
		CoHT-1, 1063 h	−8.0[8]
		CoHT-1, 2765 h	−8.1[8]
		CoHT-2, 983 h	−8.3[8]
		CoHT-2, 2687 h	−8.4[8]
		CoHT-4, 0.4 h	−10.6[8]
		CoHT-4, 33 h	−10.5[8]

[1] Nordstrom and May, 1996.
[2] Baes and Mesmer, 1986.
[3] Zachara *et al.*, 1991.
[4] Smith and Martell, 1997.
[5] Hemingway and Sposito, 1996.
[6] Nordstrom and Munoz, 1994.
[7] Naumov *et al.*, 1974.
[8] Logarithms of precipitate ion activity products (tabulated as $-\log Q_{sp}$) calculated as described in Equations (4) and (5). Equation (5) uses the uncharged aqueous silicate ion instead of the divalent silicate anion in the component set, but the formation constant for the former can be used to convert the equation.

ICP-MS (Hewlett Packard 4500). The Al concentration in many samples was below the detection limit of the instrument (1 ppb or 0.04 μM Al).

Calculation of standard error of concentration included error associated with gravimetric measurements (to increase sample volume for analysis) and the standard deviation of ICP-MS measurements. The latter error component was consistently several orders of magnitude greater than the former, based on comparisons of the ratio of the error squared to the value squared. Each error (λ_{Co}) represents a 95% confidence limit for the concentration, and was calculated as:

$$\lambda_{Co} = [Co(\mu M)]\left[\frac{\lambda_{icpms}^2}{[Co(\mu M)]_{meas}^2} + \frac{\lambda_{DF}^2}{DF_{tot}^2}\right]^{1/2} \quad (1)$$

where [Co(μM)] is the actual concentration of the analyte, in this case Co; λ_{icpms} is the error associated with the ICP-MS measurement; $[Co(\mu M)]_{meas}$ is the measured concentration of the analyte, before accounting for dilution factors; λ_{DF} is the error associated with dilution, and DF_{tot} is the dilution factor, including all parts of a serial dilution. Also,

$$\lambda_{icpms} = \frac{tS}{N^{1/2}} \quad (2)$$

where t is a tabulated constant that is a function of the number of measurements made (for N = 5, t = 2.78); S is the square root of the variance of the measurements; and N is the number of independent measurements made, in this case, 5 for each analysis.

For each dilution made, gravimetric measurements were made of the container tare (A), container + sample (B), and container + sample + diluent (C). The dilution factor for each part of the series was calculated as DF = (C − A)/(B − A) and its corresponding error, λ_{DF},

$$\lambda_{DF} = DF \times \left[\frac{2\lambda_x^2}{(C - A)^2} + \frac{2\lambda_x^2}{(B - A)^2}\right]^{1/2} \quad (3)$$

where the value of λ_x depends on the instrument, and in this case was 0.0002 g.

Ion-activity products were calculated from dissolved ion concentrations reported in Table 1 for those samples where Al analyses were reliably obtained. Ion activities were calculated from measured concentrations using the HYDRAQL program (Papelis *et al.*, 1988) and thermodynamic data listed in Table 2. Chemical equilibria for determining the products are developed below.

Samples for powder XRD were collected from experimental suspensions at 73 and 532 h (CoHT-1) and at 674 h (CoHT-4). Samples were filtered and air-dried. Depending on available sample volume, XRD patterns were collected using CuKα radiation on a Siemens diffractometer or an INEL diffractometer using an 0.1-mm glass capillary mount in Debye-Scherrer geometry. Due to limited sample volume, we were unable to obtain XRD data for CoHT-2.

TEM specimens were prepared by pipeting a drop of well-mixed suspension onto a holey C film supported by a Cu grid. TEM images and selected area diffraction (SAD) patterns were collected for CoHT-1 (74 d), CoHT-2 (33 d), and CoHT-4 (increasing pH stage and 76 h). AEM of the same specimens provided elemental information. High-resolution TEM

(HRTEM) images of CoHT-4 (170 h) were also obtained. TEM and AEM data were collected at 200 kV on a JEOL JEM 200CX equipped with a Kevex System 8000 detector and HRTEM data were collected at 300 kV on a Philips CM300, both at the National Center for Electron Microscopy, Berkeley, California.

EXAFS samples were prepared following filtration and air drying. For CoHT-1, a portion of the filter cake was mixed with boron nitride (BN) in a 1:5 precipitate: BN weight ratio and then loaded in an Al holder between Mylar windows. Because less CoHT-2 and CoHT-4 product was available, the precipitate-encrusted filter membrane was enclosed in Mylar tape without dilution.

Co K-edge (and Ni K-edge, for nepouite) EXAFS data were collected at the Stanford Synchrotron Radiation Laboratory (SSRL) on beamlines 4-2 and 4-3 using $\phi = 0$ and 90° orientations of a Si(220) crystal. Monochromator slits were set to 2 (vertical) × 20 mm (horizontal). A mirror was used to remove harmonic components of the X-ray beam. Scans were run 20–30% detuned to optimize the data for background subtraction. All data were collected at room temperature. CoHT-2 and CoHT-4 data were collected using an Ar-filled Lytle detector with Fe filter. CoHT-1 and reference structure data were collected in transmission geometry using N_2-filled ion chambers. Simultaneous collection of Co metal transmission data downstream of the sample provided a continuous energy reference for the sample spectrum.

EXAFS data were analyzed using EXAFSPAK (George and Pickering, 1995) to manipulate the data and FEFF7 (Rehr *et al.*, 1991) to calculate phase-shift and amplitude functions for fitting the data, as described previously (Thompson *et al.*, 1997). The procedure was tested on experimental EXAFS data from reference structures in which Co speciation is well known, including aqueous cobalt monomer [$Co(H_2O)_6^{2+}$] and pink cobalt hydroxide [$Co(OH)_2$(s)]. In addition, the Ni K-edge EXAFS spectrum of nepouite ($Ni_3Si_2O_5(OH)_4$) was analyzed using this procedure; the octahedral Ni site in nepouite is believed analogous to the octahedral Co site in Co-substituted serpentine. FEFF7 functions were calculated for several structures, including inactive $Co(OH)_2$ to fit aqueous cobalt monomer and pink $Co(OH)_2$ data, lizardite to fit nepouite data, and cobalt hydrotalcite to fit precipitate data. Because no structure refinement has been published for cobalt hydrotalcite, a $Co_4Al_4(OH)_{16}(CO_3)_2$ composition with the hydrotalcite structure was generated using the molecular modeling package Cerius^2 (Molecular Simulations, Inc., San Diego) by substituting a 1:1 mixture of Co and Al for all of the cations in the $Mg_6Al_2(OH)_{16}CO_3$ structure, forcing a random ordering of Co and Al on the octahedral sites. Although equimolar amounts of Co and Al are not typically found in hydrotalcites, this approach guaranteed that all possible ion-neighbor combinations would be represented in the resulting structure. The Co:Al ratio of the Cerius^2 structure in no way influenced coordination numbers resulting from the fit of EXAFS data.

In addition to individual atom-pair paths, "path groups" were included in the fit in areas of the spectrum where multiple paths overlapped in frequency space. A "path group" comprises two or more scattering contributions that are treated as a single shell for fitting purposes, and consists of multiple-scattering or combined single and multiple-scattering contributions. Using path groups has the distinct advantage of reducing the number of shells in a fit, thus potentially reducing the number of variables. Using path groups has the disadvantage of making some information inaccessible, *e.g.*, the coordination number for a path group can be a variable in a fit, but its value obscures the individual path coordination numbers. Even if coordination numbers are obscured in a fit using a path group, qualitative information about the structure and minimum size of the atom cluster remains available. Path groups used here include: 1) MS4, which consists of six three-legged paths involving nearest-neighbor O atoms, 12 four-legged paths involving nearest-neighbor O atoms, and for all except the aqueous reference sample spectrum, eight four-legged paths involving nearest-neighbor O atoms and second-neighbor Co atoms (Co1); and 2) MS6, which consists of single scattering from Co3, three- and four-legged linear multiple scattering through Co1 to Co3, and a large number of three-legged, non-linear multiple-scattering paths involving various O atoms. The "Co#" notation (*e.g.*, Co1, Co2 . . .) is explained in the caption for Figure 1.

RESULTS

Size and morphology

Bright-field TEM images of precipitates from aged (>1000 h) CoHT-1 and CoHT-2 suspensions show ragged, micron-sized particles (Figure 2). SAD patterns indicate a polycrystalline material. Dark-field imaging techniques, which display only those particles oriented in a particular direction, reveal that the micron-sized aggregates are composed of nanoscale (2 to 5-nm diameter) particles.

Particle aggregates were not commonly found in images of CoHT-4 aged in suspension up to 170 h. Instead, nanoscale particles were indicated by lattice fringes that lined the amorphous support web in high-resolution images (Figure 3). If the spatial extent of a continuous set of lattice fringes corresponds to a single precipitate particle, then CoHT-4 precipitates are 2–10 nm in diameter after 170 h.

Structure

The CoHT-1 precipitates are isostructural with hydrotalcite. The positions and relative intensities of

https://doi.org/10.1346/CCMN.1999.0470405 Published online by Cambridge University Press

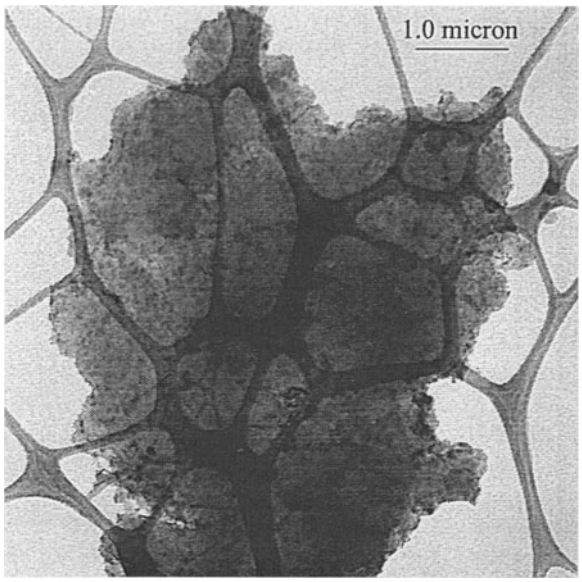

Figure 2. TEM bright-field image of CoHT-2 particle cluster after 33 d. Individual particles that constitute the cluster are ~2–5 nm in diameter.

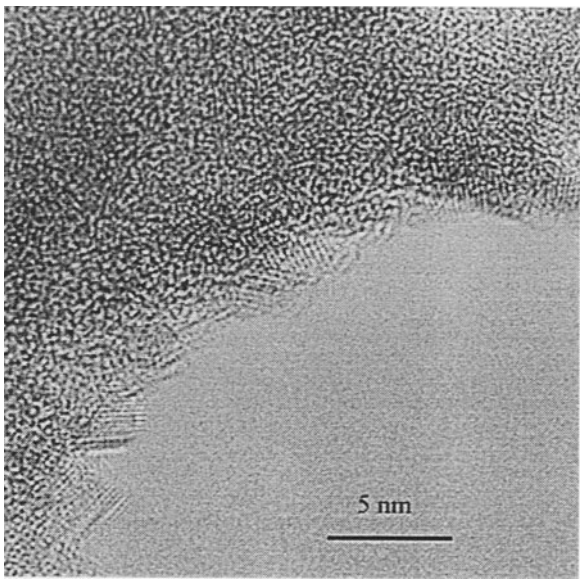

Figure 3. HRTEM image of CoHT-4 precipitates after 170 h. Image shows holey C support (upper left, darker area) decorated by lattice fringes along the lower right edge of support. Fringe spacings are due to CoHT precipitates.

CoHT-1 powder XRD reflections (Figure 4) match those reported for a crystalline Co-Al hydroxycarbonate, which is isostructural with hydrotalcite (Busca *et al.*, 1992). Rietveld refinement of the CoHT-1 pattern, which has considerable structure out to 150 °2θ, produces lattice parameters of a = 3.0752(4) and c = 22.891(6) based on hexagonal ($R\bar{3}m$) symmetry. Powder XRD peaks for CoHT-1 are broadened, consistent with small particle sizes observed by TEM. Rietveld refinement also indicates a considerable amount of strain broadening of peaks, probably owing to inhomogeneities in the sample. Powder XRD patterns for the two CoHT-1 precipitates are indistinguishable, suggesting the precipitate did not change significantly between 73–532 h.

On their own, powder XRD results for CoHT-4 are inconclusive. Attempts to obtain powder XRD data for CoHT-4, by using either a glass capillary or Mylar tape, produced primarily a broad, slightly asymmetric 7.2-Å reflection amidst broader, less intense peaks from the mounting material. The 7.2-Å spacing is smaller by at least 0.3 Å than d(003) for hydrotalcite-like phases containing nitrate, carbonate, and hydroxide interlayers (Bish, 1980). The few CoHT-4 d-values from HRTEM images correspond to non-basal diffraction peaks reported for hydrotalcite-like phases (Schutz and Biloen, 1987; Hansen *et al.*, 1994).

EXAFS spectra for the three precipitates suggest that they are locally isostructural with hydrotalcite (Figure 5). Spectral fits (Table 3) include contributions from nearest O atom neighbors, Co1 and Al at 3.1 Å, a 4.2-Å multiple-scattering path group (MS4), Co2 at 5.3 Å, and a 6.2-Å single-plus-multiple-scattering path group (MS6). The average Co atom in the precipitates has six O nearest neighbors, four to six Co1 second neighbors with zero to two Al second neighbors at the same distance, two to five Co2 neighbors, and an undetermined but nonzero number of Co3 neighbors. Coordination number and distance information for Co in the precipitates describe the local atomic environment for divalent metals in hydrotalcites. Compared with typical hydrotalcite stoichiometries, small Co2 coordination numbers in the precipitates probably result from small precipitate particles, and small Al coordination numbers are attributable to weak X-ray scattering by Al. The absence of an Al contribution from the CoHT-4 Co1 shell suggests less Al is present in the CoHT-4 precipitate than in the CoHT-1 and CoHT-2

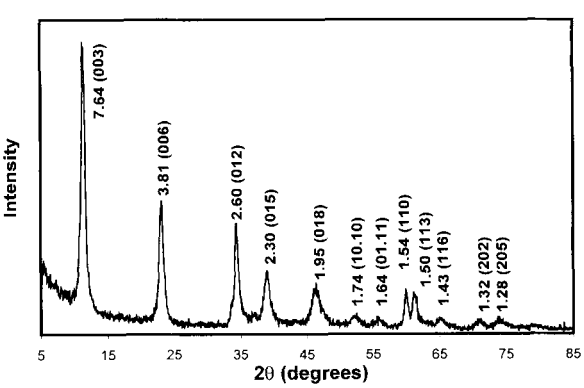

Figure 4. Powder XRD pattern for CoHT-1 at 73 h. d-value (Å) and Miller index (in parentheses) appear above each peak.

https://doi.org/10.1346/CCMN.1999.0470405 Published online by Cambridge University Press

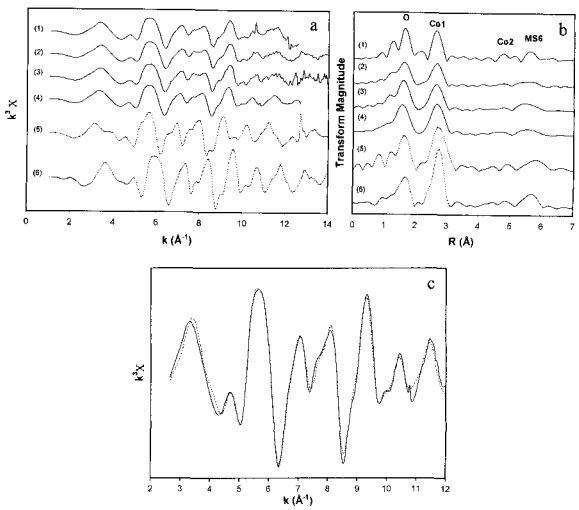

Figure 5. a) EXAFS spectra and b) Fourier transforms. Solid lines are precipitate spectra; dashed lines are reference structure spectra. (1) CoHT-1, 73 h (2) CoHT-2, 16 h (3) CoHT-2, 451 h (4) CoHT-4, 674 h (5) $Co(OH)_2$, and (6) nepouite. Major peaks are labeled in b) with neighboring atom shell designation, at top. c) Representative data fit for CoHT-4, consistent with fit parameters in Table 3.

precipitates, resulting in a lower layer charge for CoHT-4.

CoHT-1 precipitates may have Co- and Al-rich domains, rather than local cation ordering driven by Al avoidance (Vucelic *et al.*, 1997) or random cation ordering (Cavani *et al.*, 1991). The symmetry of hydrotalcites requires that the *a* cell parameter be equal to the cation-cation distance, assuming random ordering of the cations. A larger Co-Co distance (3.10 Å), as found by Co EXAFS for CoHT-1, is consistent with clustering of Co atoms, producing local interatomic distances more similar to pure $Co(OH)_2$, in which the distance between Co second neighbors is 3.17 Å. In contrast, XRD measures the average lattice parameter (a = 3.0752(4) Å) for the entire (Co,Al) hydroxide structure, and this is influenced by both the Co cluster and the smaller $Al(OH)_3$-like cluster. Where clustering of similar cations occurs, the XRD-derived value of *a* is therefore smaller than the cation-cation distance derived from EXAFS spectroscopy. Clustering of Co and Al atoms is also consistent with the strain broadening found by Rietveld refinement of the powder XRD pattern. Differences between the *a* cell parameter from XRD and the cation-cation distance from EXAFS data were also reported for takovite (Scheidegger *et al.*, 1998), the Ni-Al analog of hydrotalcite, but not for pyroaurite, the Mg-Fe(III) analog (Vucelic *et al.*, 1997). Cation clustering and the associated discrepancy between XRD lattice parameters and EXAFS interatomic distances may be a consequence of strain arising from significant differences in ionic radius between the two cations occupying the hydroxide layers of hydrotalcite-like phases, as for Co(II), r = 0.735 Å and Al(III), r = 0.530 Å); and Ni(II), r = 0.700 Å, and Al(III); but not Mg(II), r = 0.720 Å, and Fe(III), r = 0.645 Å (Shannon and Prewitt, 1969). Without XRD data of high quality for CoHT-2 and CoHT-4, similar analyses cannot be made for those precipitates.

Combined with the XRD and HRTEM data, the EXAFS data suggest that CoHT-4 particles are interstratified hydrotalcites, with hydroxide layers incompletely separated by anionic interlayers. The low hydroxide layer charge requires a low anion content. Because EXAFS spectroscopy provides local information only, it is incapable of distinguishing between the Co environment in an interstratified hydrotalcite and that in a normal hydrotalcite. Interstratification commonly produces XRD *d*(00*l*) peaks that are broadened and located at an intermediate position between those of the two end-members, as found in XRD patterns of Mn and Ni-containing hydrotalcites with incomplete interlayers (Guerlou-Demourgues *et al.*, 1994) and Ni-Fe hydrotalcites with low layer charge (Refait and Genin, 1997). The basal spacing for hydrotalcite with a complete interlayer is ≥7.5 Å, whereas the corresponding spacing in $Co(OH)_2$, the nearest end-member, is 4.64 Å (Lotmar and Feitknecht, 1936). The 7.2-Å peak found in the CoHT-4 powder pattern is therefore consistent with incomplete separation of Co and Al-containing hydroxide layers by anionic interlayers in CoHT-4.

Composition

Combined data sources indicate an average stoichiometry of 3Co:Al for CoHT-1 and CoHT-2, consistent with other hydrotalcite compositions (Cavani *et al.*, 1991). AEM of aged (>1000 h) CoHT-1 and CoHT-2 precipitates detected two to three Co atoms per Al atom. Cumulative losses of Co and Al from solution (Figures 6 and 7) suggest a bulk solid-phase stoichiometry of 3.3Co:Al for CoHT-1; the CoHT-2 solution data are too noisy for a determination of stoichiometry. Precipitate Co:Al ratios calculated from the magnitude of the lattice parameter *a* (Brindley and Kikkawa, 1979) are 3.3 (CoHT-1) and 3.3–4.1 (CoHT-2), based on tabulated Co(II) and Al(III) radii (Shannon and Prewitt, 1969), *a* from Rietveld analysis for CoHT-1, and the Co-Co1 interatomic distance from EXAFS as an alternative measure of *a* for CoHT-2.

Based on solution data, the bulk solid-phase stoichiometry in the CoHT-4 experiment evolved from two to five Co atoms per Al atom during the 170-h experiment. The change arose from continued Co uptake after dissolved Al was depleted. Cobalt adsorption on precipitate surfaces is consistent with Co uptake without Al uptake, but Co surface adsorption is rapid (Hachiya *et al.*, 1984), in contrast to the gradual uptake observed (Figure 8a). Precipitation of an increasingly Co-rich hydrotalcite, ultimately containing

Table 3. EXAFS spectra fit results and XRD reference data. Coordination number (N), interatomic distance (R), and Debye-Waller disorder parameter (σ^2) for each shell of atom neighbors; spectrum energy shift in eV relative to FEFF reference (ΔE_0).

		O			Co1			Misc.	
Sample	Age[2]	N	R (Å)	σ^2 (Å^2)	N	R (Å)	σ^2 (Å^2)	Path	N
CoHT-1	73	6	2.09	0.007	5.4	3.10	0.009	Al[3]	0.6
CoHT-2	16	6	2.10	0.009	4.7	3.10	0.009	Al	1.3
CoHT-2	451	6	2.10	0.008	4.7	3.11	0.009	Al	1.3
CoHT-4	674	6	2.08	0.008	5.6	3.11	0.009	MS[4]	1.5
Reference									
$Co(OH)_2$		6	2.10	0.006	6	3.19	0.006		
Nepouite[5]		3	2.02	0.003	6	3.07	0.005	Si	2
		1	2.07	0.002					
		2	2.14	0.004					
XRD									
Cobalt HT[6]						3.08		Al	
HT[7]		6	2.02		4	3.05		Al	2
Pyroaurite[7]		6	2.06		4	3.11		Fe	2
$Co(OH)_2$		6	2.09		6	3.17			

[1] MS6 path group, described in the text, which includes Co3. The presence of MS6 shell information indicates that Co2 is likely present, even if not detected.

[2] Precipitate age in hours corresponds to time at which sample was harvested from synthesis vessel.

[3] The Al contribution is weak, thus Al may be overlooked in the fit, even when Al atoms are present. Co1 coordination numbers of 5 or fewer suggest Al probably occupies one or more positions in the Co1 shell. To include Al, $R_{Co\text{-}Al}$ must be equal to $R_{Co\text{-}Co1}$.

[4] MS4 path group, described in text. MS4 contribution was included in every fit except CoHT-2, 451 h, but is only shown for CoHT-4 due to space limitations. The MS4 contribution cannot always be discerned because it is strongest in a busy area of the spectrum.

[5] For nepouite, Ni is the central absorbing atom and Ni atom neighbors occupy Co positions in the table.

[6] Cobalt hydrotalcite.

[7] Hydrotalcite (HT) and pyroaurite are Mg-Al and Mg-Fe(III) analogs of the layered double hydroxide structure, respectively. For HT, substitute Mg for Co; for pyroaurite, substitute Mg for Co and Fe(III) for Al relative to CoHT.

Structure references: $Co(OH)_2$ (Lotmar and Feitknecht, 1936); Lizardite/nepouite (Rucklidge and Zussman, 1965); Cobalt hydrotalcite (Busca *et al.*, 1992); Hydrotalcite (Allmann and Jepsen, 1969); Pyroaurite (Allmann, 1968).

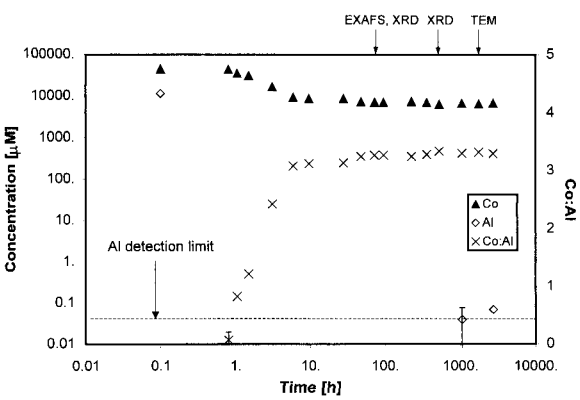

Figure 6. CoHT-1 ion concentrations and bulk solid-phase ion ratios *vs.* time. Bulk solid-phase ratio is calculated as (cumulative change in dissolved Co)/(cumulative change in dissolved Al). Data were collected at pH 6.9. Error bars are smaller than data symbols, unless shown. Time = 0 is defined as the time at which Co and Al solutions were mixed. Data for Al and Co concentrations plotted at 0.1 h were measured on separate solutions, prior to mixing. All other data were collected post-mixing and are plotted at the appropriate time relative to mixing. Missing Al concentration data indicate concentrations at or below the Al detection limit. Arrows at top indicate times of sample collection for the specified analysis.

five Co atoms per Al atom, more likely accounts for the excess Co uptake. The calculation of mole fraction from lattice parameter, described above, indicates a ratio of 4.1 Co atoms per Al atom for the CoHT-4 precipitate harvested after 674 h. This relatively high Co:Al ratio and therefore low layer charge is consistent with XRD results that indicate an incomplete anionic interlayer. Because Al was depleted from solution well before the Co-rich stoichiometry was achieved, dissolution of the previously formed precipitate was necessary to provide Al for precipitation of the Co-enriched solid; the dissolution-reprecipitation sequence can account for the sluggishness of later-stage Co uptake.

Carbonate dominates the CoHT-1 interlayer and probably dominates the CoHT-2 interlayer, consistent with findings that double hydroxides synthesized in air routinely have carbonate interlayers (Bish, 1980). The 2θ value (12°) of the (003) reflection in the CoHT-1 XRD pattern (Figure 4) is consistent with a divalent carbonate interlayer (7.35–7.50 Å). Nitrate interlayers have been assigned to *d*(003) values between 7.50 Å (Bish, 1980) and 8.35 Å (Miyata, 1983), and therefore cannot be ruled out absolutely for CoHT-1. Carbonate added directly to the CoHT-1 experiment as Na_2CO_3

https://doi.org/10.1346/CCMN.1999.0470405 Published online by Cambridge University Press

Table 3. Extended.

Misc.		Co2			MS6[1]			
R (Å)	σ^2 (Å^2)	N	R (Å)	σ^2 (Å^2)	N	R (Å)	σ^2 (Å^2)	ΔE_0
3.10	0.002	3.5	5.35	0.009	1.5	6.21	0.008	−2.1
3.10	0.013	2.3	5.34	0.007	1.5	6.22	0.009	−0.7
3.11	0.014				1.8	6.24	0.010	−0.4
4.20	0.007	5.5	5.34	0.012	1.9	6.23	0.010	−4.1
		6	6.35	0.027				+0.1
3.29	0.004	5.3	5.32	0.009				−0.8
3.08								
3.05		4	5.29		4	6.11		
3.11		4	5.38		4	6.22		
		6	6.35					

was ten times that required to fix all Al present in a carbonate-containing hydrotalcite phase, however. In contrast, carbonate was introduced into the CoHT-2 experiment only by diffusion from air. The CoHT-2 reaction vessel was continuously open and stirred for the first 16 h, therefore sufficient carbonate to occupy precipitate interlayers may have dissolved in the experimental solution.

Indirect information suggests that silicate, as monovalent $H_3SiO_4^-$, occupied the CoHT-4 precipitate interlayer increasingly with time. Possible interlayer anions include only NO_3^-, OH^-, and $H_3SiO_4^-$or $H_2SiO_4^{2-}$ in this system (carbonate was excluded). Based on concentration alone, NO_3^- should dominate the interlayer. But the dissolved Si concentration decreased with time in an amount equivalent to the layer charge of the precipitate, assuming monovalent silicate uptake (Figure 8b and 8c), and incorporation of silicate into the precipitate is the only plausible explanation. Precipitation of a discrete, Si-containing phase was unlikely, as the system was undersaturated with respect to SiO_2 polymorphs and all silicates for which there are known solubility products. Furthermore, the EXAFS spectrum of the precipitate indicates a short-range Co environment that is distinctly different from the Ni environment in nepouite (Table 3). Therefore, silicate is the dominant interlayer anion in CoHT-4 precipitates. Because $H_3SiO_4^-$ is much more abundant than $H_2SiO_4^{2-}$ under experimental conditions and the former does not readily deprotonate, interlayer silicate should be in the form of $H_3SiO_4^-$, rather than $H_2SiO_4^{2-}$. In CoHT-4, silicate anions do not form continuous interlayers, rather, hydroxide layers are collapsed together in some areas, as discussed above.

Solubility product

The compositional and structural information suggest the following precipitate stoichiometries: $Co_{0.75}Al_{0.25}(OH)_2(CO_3)_{0.125}$ (CoHT-1 and CoHT-2) and $Co_{0.83}Al_{0.17}(OH)_2(H_3SiO_4)_{0.17}$ (CoHT-4). The Co:Al stoichiometry of CoHT-1 and CoHT-2 is an average of values from AEM, solution, and crystallographic data. The Co:Al stoichiometry of CoHT-4 is derived from late-stage solution data. We assumed a homogeneous interlayer occupied by water and the anion for which we have the strongest evidence (CO_3^{2-} in CoHT-1 and CoHT-2, $H_3SiO_4^-$ in CoHT-4). Because interlayer anion identities were determined indirectly, we cannot rule out a mixture of anions in the interlayer. Anion stoichiometry was fixed to x/n, where x is Al mole fraction and n is anion charge. Hydroxide-ion stoichiometry was used to balance the formula. From reaction equilibria

$$Co_{0.75}Al_{0.25}(OH)_2(CO_3)_{0.125}(s) + 2H^+(aq) \leftrightarrow 0.75Co^{2+}(aq) + 0.25Al^{3+}(aq) + 0.125CO_3^{2-}(aq) + 2H_2O \quad (4)$$

for CoHT-1 and CoHT-2, and

$$Co_{0.83}Al_{0.17}(OH)_2(H_3SiO_4)_{0.17}(s) + 2.17H^+(aq) \leftrightarrow 0.83Co^{2+}(aq) + 0.17Al^{3+}(aq) + 0.17Si(OH)_4^0(aq) + 2H_2O \quad (5)$$

for CoHT-4, ion activity products (Q_{sp}) were calculated from solution data (Table 2). Unchanging cobalt concentrations and ion-activity products indicate an apparent steady state was achieved late in the CoHT-1 and CoHT-2 experiments, suggesting those ion-activity products may approximate equilibrium solubility products. Cobalt concentrations did not stabilize in the much shorter CoHT-4 experiment, therefore the ion-

https://doi.org/10.1346/CCMN.1999.0470405 Published online by Cambridge University Press

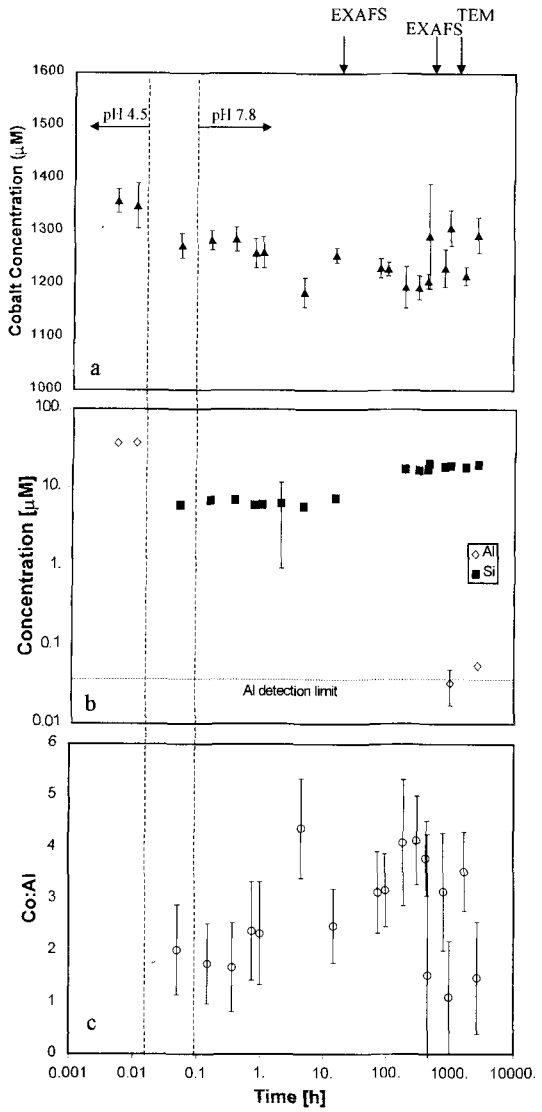

Figure 7. CoHT-2 ion concentrations and bulk solid-phase ion ratios *vs.* time. (a) dissolved Co, (b) dissolved Al and Si, and (c) bulk solid-phase Co:Al ratio, calculated as described in Figure 6 caption. Solution pH increased with time, with vertical dashed lines separating regions of pH 4.5, increasing pH, and pH 7.8 from left to right. Error bars are smaller than data symbols, unless shown. Time = 0 is defined as the time at which pH 7.8 was first achieved in the mixed solution. Data plotted at 0.05 h were collected from separate Co and Al solutions prior to mixing, those plotted at 0.1 h were collected just after mixing, and those plotted at 0.6 h were collected at pH 7.1 while pH was increasing. All other data were collected at pH 7.8 and are plotted at the appropriate time relative to achieving pH 7.8. Missing Al concentration data indicate concentrations at or below the Al detection limit. Arrows at top indicate times of sample collection for the specified analysis.

activity products reported for CoHT-4 are not equilibrium solubility products. Decreasing Co concentrations in the CoHT-4 experiment suggest the CoHT-4 equilibrium solubility product (K_{sp}) is smaller than the absolute value of CoHT-4 ion-activity products (Q_{sp}) reported in Table 2.

Possible impurity phases

Using solubility and ion-activity products reported in Table 2, we calculated the saturation state of the solutions at each stage of the experiments. Under final pH conditions, Co hydrotalcite phases are the only stable solids. Prior to mixing, however, separate CoHT-1 solutions were highly supersaturated with respect to $CoCO_3$ and amorphous $Al(OH)_3$. Precipitation in each solution was verified with laser scattering, and the low early Co:Al uptake ratios suggest that much more $Al(OH)_3$ formed than $CoCO_3$. Dissolution of these phases necessarily preceded CoHT precipitation in CoHT-1. The CoHT-2 and CoHT-4 solutions also reached supersaturation with respect to $Al(OH)_3$ phases as pH was increased: the CoHT-4 solution was supersaturated with respect to amorphous $Al(OH)_3$, which precipitates rapidly (Hemingway and Sposito, 1996), and several crystalline $Al(OH)_3$ phases, but the CoHT-2 solution only exceeded saturation with respect to the less soluble, crystalline forms of $Al(OH)_3$. Aluminum hydroxide precipitation probably caused the laser scattering that was observed at pH 5.3 in CoHT-4, consistent with early Co:Al uptake ratios that are lower than later ratios, but the $Al(OH)_3$ precipitate dissolved a short time later to allow CoHT precipitation. Laser scattering at pH 7, but not lower, in CoHT-2 may be evidence for CoHT precipitation without prior $Al(OH)_3$ precipitation.

Reaction rates

Qualitative information on reaction rates is derived from ion-loss rates and EXAFS data. In CoHT-2 and CoHT-4 experiments, Co and Al were removed from solution in quantities consistent with CoHT precipitation within the first hour. In a separate experiment, X-ray absorption near-edge spectra collected in real time from an experiment identical to that in which CoHT-2 was produced indicate the formation of a hydrotalcite-like local Co environment within two hours (Thompson, unpublished). These data suggest that CoHT precipitation from dissolved reactants occurs on the time scale of minutes. In contrast, CoHT-1 ion loss took longer to achieve the hydrotalcite ratio (average 3Co:Al). Because ion mixing followed pH adjustment in the CoHT-1 experiment, $Al(OH)_3$ and $CoCO_3$ impurity phases formed, making Al and Co release by dissolution the rate-limiting steps for CoHT formation. Dissolution of CoHT formed early in the CoHT-4 ex-

https://doi.org/10.1346/CCMN.1999.0470405 Published online by Cambridge University Press

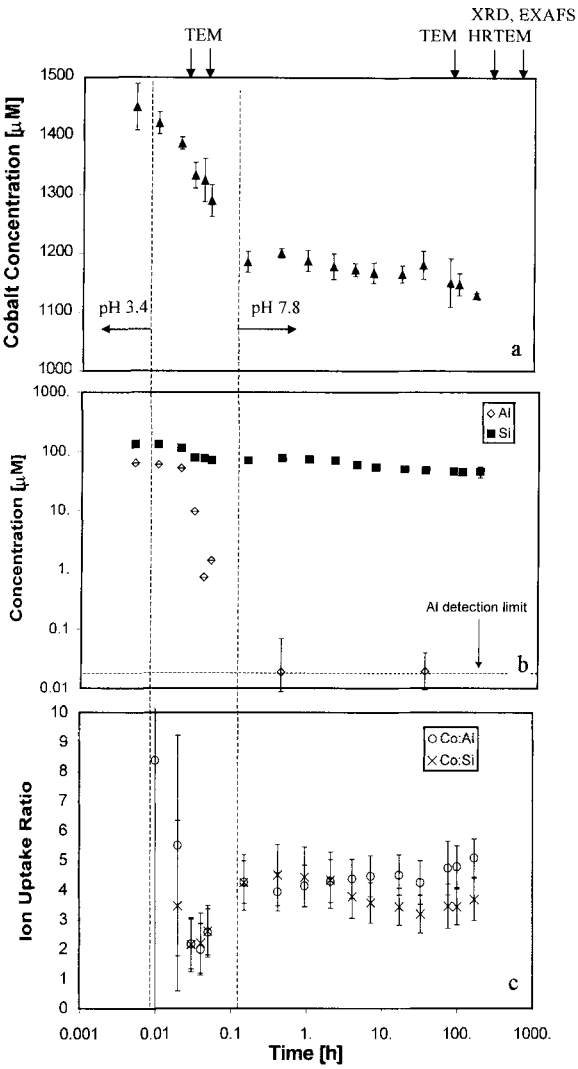

Figure 8. CoHT-4 ion concentrations and bulk solid-phase ion ratios *vs.* time. (a) Dissolved Co, (b) dissolved Al and Si, and (c) bulk solid-phase Co:Al and Co:Si ratios, calculated as described in Figure 6 caption. Solution pH increased with time, with vertical dashed lines separating regions of pH 3.4, increasing pH, and pH 7.8 from left to right. Error bars are smaller than data symbols, unless shown. All data were collected from mixed solution containing Co, Al, and Si; those data plotted before 0.1 h were collected prior to reaching pH 7.8 (time = 0). Missing Al concentration data indicate concentrations at or below the Al detection limit. Arrows at top indicate times of sample collection for the specified analysis.

periment similarly limited subsequent precipitation of the Co-enriched hydrotalcite.

DISCUSSION

Cobalt hydrotalcites precipitated homogeneously in the experiments, and have the general form $[Co(II)_{1-x}Al(III)_x(OH)_2]^{x+}(A^{n-}_{x/n})\cdot mH_2O$, with $x = 0.17$ to 0.25, $n = 1$ or 2, and m undetermined. Monovalent silicate ions ($A = H_3SiO_4^-$) occupy the CoHT-4 interlayer, whereas divalent carbonate ions ($A = CO_3^{2-}$) occupy the interlayers of CoHT-1 and CoHT-2. The mole fraction of Al in the precipitate is independent of the mole fraction of Al in the system, but depends on solution composition through interlayer anion charge. For example, the CoHT-4 precipitate has a smaller Al mole fraction (0.17) than the CoHT-2 precipitate (0.25). Both were precipitated from solutions containing similar concentrations of Co and Al, but divalent carbonate in CoHT-2 effectively balanced the layer charge attributable to Al (Miyata, 1983), whereas the absence of divalent anions in CoHT-4 probably promoted the lower Al mole fraction.

Precipitate stoichiometries were established for each experiment to estimate solubility products, but hydrotalcite compounds may, in fact, behave as a solid-solution series of $[Co(II)_{1-x}Al(III)_x(OH)_2]^{x+}(A^{n-}_{x/n})\cdot mH_2O$. Although the structures of $Co(OH)_2$ and gibbsite $[Al(OH)_3]$ are similar, their cell parameters differ considerably, therefore it is not surprising that the range of hydrotalcite stoichiometries does not extend between these two more distant end-members (Navrotsky, 1994). Based on this study alone, the compositional range for complete solid solution is limited to $0.17 < x \leq 0.25$, but hydroxide layer collapse occurred for $x = 0.17$ and clustering of similar cations occurred in at least one CoHT. Solid-solution behavior may therefore be complete only on a macroscopic scale, whereas molecular-scale inhomogeneities may be present for all CoHT stoichiometries. Alternatively, $[Co(II)_{1-x}Al(III)_x(OH)_2]^{x+}(A^{n-}_{x/n})\cdot mH_2O$ may not be a solid-solution series at all, but a family of distinct compounds. In either case, our results suggest that CoHT can have a variable Co(II):Al(III) stoichiometry.

Variable stoichiometry has two important implications. First, although a single final stoichiometry was assumed for each experiment, the probability of a broader range of stoichiometries indicates that our solubility products are only approximations when applied to a range of solution compositions. Second, stability varies with stoichiometry. It follows from Equations (4) and (5) that for a fixed system Co concentration, the most stable CoHT stoichiometry varies with pH. Conversely, for fixed pH, the most stable stoichiometry varies with Co concentration.

Cobalt hydrotalcites formed from ions from several sources: dissolved Co, Co from $CoCO_3$ (CoHT-1 only), and Co from CoHT formed earlier; dissolved Al, Al from $Al(OH)_3$, and Al from CoHT formed earlier. Precipitation directly from dissolved ions was rapid, whereas precipitation via a solid phase was slow. Protons were released in each case, as illustrated by the following net reactions:

https://doi.org/10.1346/CCMN.1999.0470405 Published online by Cambridge University Press

$$0.75Co^{2+}(aq) + 0.25Al^{3+}(aq) + 0.25/nA^{n-}(aq) + 2H_2O \leftrightarrow Co_{0.75}Al_{0.25}(OH)_2A_{0.25/n}(s) + 2H^+(aq) \quad (6)$$

$$0.75Co^{2+}(aq) + 0.25Al(OH)_3(s) + 0.25/nA^{n-}(aq) + 1.25H_2O \leftrightarrow Co_{0.75}Al_{0.25}(OH)_2A_{0.25/n}(s) + 1.25H^+(aq) \quad (7)$$

$$Co_{0.75}Al_{0.25}(OH)_2A_{0.25/n}(s) + 0.5Co^{2+}(aq) + H_2O \leftrightarrow Co_{1.25}Al_{0.25}(OH)_3A_{0.25/n}(s) + H^+(aq). \quad (8)$$

These reactions require that cobalt hydrotalcites precipitate above a pH threshold dependent on Co, Al, and anion concentrations. This threshold is near pH 7.0 in the experiments reported here, and is slightly lower if $Al(OH)_3$ precipitation does not occur.

Above a higher pH threshold, $Co(OH)_2$ or $CoCO_3$ is the dominant sink for Co, as illustrated by the following reactions:

$$Co_{0.75}Al_{0.25}(OH)_2A_{0.25/n}(s) + 0.25H_2O \leftrightarrow 0.75Co(OH)_2(s) + 0.25Al(OH)_3(s) + 0.25/nA^{n-}(aq) + 0.25H^+(aq) \quad (9)$$

$$Co_{0.75}Al_{0.25}(OH)_2(CO_3)_{0.125}(s) + 0.25H_2O \leftrightarrow 0.125CoCO_3(s) + 0.625Co(OH)_2(s) + 0.25Al(OH)_4^-(aq) + 0.25H^+(aq). \quad (10)$$

The threshold with CoHT is at pH 7.9 for $Co(OH)_2$ in CoHT-4, at pH 7.5 for $CoCO_3$ in CoHT-2, and at pH 7.1 for $CoCO_3$ in CoHT-1. This implies a small window for CoHT as the sole Co solid phase. Above the threshold, CoHT coexists as a minor phase with the hydroxide solid until pH 11 or with the carbonate solid until pH 9. Although experimental conditions crossed this pH threshold in CoHT-2, there was no evidence for $CoCO_3$ precipitation.

Aluminum availability limited the rate and extent of CoHT precipitation. It follows from Equations (6) through (10) that larger Al concentrations will increase the pH range over which CoHT is stable. We expect that Al may similarly limit CoHT formation in nature. Because CoHT formed at the expense of Al-rich phases in the experiments, the same may occur in nature. Aluminum-rich phases formed rapidly in the experiments and were likely amorphous, whereas naturally occurring phases may form over time and stabilize. Slower precursor dissolution would slow CoHT precipitation in nature relative to the rates observed here. Cobalt-uptake rates observed in the middle of the CoHT-1 experiment may provide an upper limit for the rate of Co uptake by CoHT formation in nature. In another paper (Thompson *et al.*, 1999), we report on batch sorption experiments in which CoHT forms at the expense of well-ordered kaolinite [$Al_2Si_2O_5(OH)_4$].

Ferric iron-containing hydrotalcites may provide an additional sink for Co(II) and other divalent metals released into the environment (Cavani *et al.*, 1991). Mn(II)-Fe(III) and Ni(II)-Fe(III) double hydroxides were found as coatings on river sediments (Subramanian, 1973). By analogy with Al, low Fe(III) solubility near neutral pH suggests that the rate of Fe(III) mineral dissolution will limit divalent metal uptake rates by Fe(III)-containing hydrotalcite precipitation. Indeed, laboratory experiments conducted over one year showed evidence at elevated pH for the gradual conversion of ferrihydrite to pyroaurite, the Mg-Fe(III) hydrotalcite analog (Baltpurvins *et al.*, 1997).

Finally, the small particle size of the CoHT precipitates raises the issue of contaminant mobility. Because individual crystallites fit the size definition of a colloid, hydrotalcite particles might be transported as suspended matter at total metal concentrations exceeding hydrotalcite solubility in water. We see evidence for aggregation of nanoscale precipitate particles after hundreds of hours in the precipitation experiments, and this might retard transport, if transport time scales are longer than aggregation time scales.

CONCLUSIONS

Cobalt hydrotalcite (CoHT) precipitated from dilute aqueous solutions with an apparent range of stoichiometries described by $[Co(II)_{1-x}Al(III)_x(OH)_2]^{x+}(A^{n-}_{x/n})\cdot mH_2O$, with x = 0.17–0.25 and A = CO_3^{2-}, NO_3^-, or $H_3SiO_4^-$. The value of x is dictated more by the anion (A) than by the mole fraction of Al in the mother solution. The amount of CoHT precipitated was limited by total Al in solution, however. Over the range of x values observed, the precipitates behaved as a solid solution from the standpoint of macroscopic composition, but molecular scale inhomogeneities were apparent. Cobalt ions clustered together in at least one CoHT product, instead of distributing evenly throughout hydroxide layers. For x = 0.17, interlayer anion content was insufficient to separate all hydroxide layers, resulting in interstratification of hydrotalcite layers that contain anion interlayers with brucite-like layers that lack interlayers. Cobalt hydrotalcite is the dominant stable phase over a narrow, near-neutral pH range for solutions containing approximately millimolar Co and micromolar Al concentrations. In that pH range, CoHT forms at the expense of poorly ordered aluminum hydroxide. At lower pH, Al is more stable as $Al(OH)_3$ and Co remains in solution or sorbs to solids. At higher pH, Co is more stable as a pure hydroxide or carbonate solid. The narrow stability range combined with nanoscale particle sizes may explain why hydrotalcite phases are infrequently observed in nature.

ACKNOWLEDGMENTS

We thank C. Echer and Y.-C. Wang for conducting TEM analyses at NCEM, LBNL and S. Chipera for the CoHT-4

powder XRD pattern. The research and manuscript benefited from input by W.H. Casey. Discussions with D. Bish helped clarify the CoHT-4 structure. Comments from S. Fendorf and an anonymous reviewer improved the manuscript. This work was funded by the Office of Basic Energy Sciences, Department of Energy (OBES-DOE) (Grant DE-FG03-93ER14347-A007) and an NSF Graduate Research Fellowship. EXAFS data were collected at SSRL, which is operated by OBES-DOE and supported by the National Institutes of Health.

REFERENCES

Allmann, R. (1968) The crystal structure of pyroaurite. *Acta Crystallographica,* **B24,** 972–977.

Allmann, R. (1970) Doppelschichtstrukturen mit brucitahnlichen schichtionen $[Me(II)_{1-x}Me(III)_x(OH)_2]^{x+}$. *Chimia,* **24,** 99–108.

Allmann, R. and Jepsen, H.P. (1969) Die struktur des hydrotalkits. *Neues Jahrbuch für Mineralogie Monatshefte,* 544–551.

Baes, C.F., Jr. and Mesmer, R.E. (1986) *The Hydrolysis of Cations.* John Wiley & Sons, New York, 489 pp.

Baltpurvins, K.A., Burns, R.C., and Lawrance, G.A. (1997) Effect of Ca^{2+}, Mg^{2+}, and anion type on the aging of iron(III) hydroxide precipitates. *Environmental Science & Technology,* **31,** 1024–1032.

Bennett, D.G., Read, D., Atkins, M., and Glasser, F.P. (1992) A thermodynamic model for blended cements. II. Cement hydrate phases: Thermodynamic values and modelling studies. *Journal of Nuclear Materials,* **190,** 315–325.

Bish, D.L. (1980) Anion-exchange in takovite: Applications to other hydroxide minerals. *Bulletin de Mineralogie,* **103,** 170–175.

Boclair, J.W. and Braterman, P.S. (1999) Layered double hydroxide stability. Part I: Relative stabilities of layered double hydroxides and their simple counterparts. *Chemistry of Materials,* **11,** 298–302.

Boclair, J.W., Braterman, P.S., Jiang, J., Lou, S., and Yarberry, F. (1999) Layered double hydroxide stability. Part II: Formation of Cr(III)-containing layered double hydroxides directly from solution. *Chemistry of Materials,* **11,** 303–307.

Brindley, G.W. and Kikkawa, S. (1979) A crystal-chemical study of Mg,Al and Ni,Al hydroxy-perchlorates and hydroxy-carbonates. *American Mineralogist,* **64,** 836–843.

Bruno, J., Duro, L., de Pablo, J., Casas, I., Ayora, C., Delgado, J., Gimeno, M.J., Pena, J., Linklater, C., Perez del Villar, L., and Gomez, P. (1998) Estimation of the concentrations of trace metals in natural systems. The application of codissolution and coprecipitation approaches to El Berrocal (Spain) and Pocos de Caldas (Brazil). *Chemical Geology,* **151,** 277–291.

Busca, G., Lorenzelli, V., and Bolis, V. (1992) Preparation, bulk characterization and surface chemistry of high-surface-area cobalt aluminate. *Materials Chemistry and Physics,* **31,** 221–228.

Cavani, F., Trifiro, F., and Vaccari, A. (1991) Hydrotalcite-type anionic clays: Preparation, properties and applications. *Catalysis Today,* **11,** 173–301.

Crovisier, J.L., Fritz, B., Grambow, B., and Eberhart, J.P. (1986) Dissolution of basaltic glass in seawater: Experiments and thermodynamic modelling. In *Scientific Basis for Nuclear Waste Management, Volume 50,* L.O. Werme, ed., Materials Research Society, Pittsburgh, 273–280.

d'Espinose de la Caillerie, J.-B., Kermarec, M., and Clause, O. (1995) Impregnation of γ-alumina with Ni(II) or Co(II) ions at neutral pH: Hydrotalcite-type coprecipitate formation and characterization. *Journal of the American Chemical Society,* **117,** 11471–11481.

Farley, K.J., Dzombak, D.A., and Morel, F.M.M. (1985) A surface precipitation model for the sorption of cations on metal oxides. *Journal of Colloid and Interface Science,* **106,** 226–242.

Feitknecht, W. (1942) Uber die bildung von doppelhydroxyden zwischen zwei- und dreiwertigen metallen. *Helvetica Chimica Acta,* **25,** 555–569.

George, G.N. and Pickering, I.J. (1995) EXAFSPAK: A suite of computer programs for analysis of x-ray absorption spectra. Stanford Synchrotron Radiation Laboratory, Stanford, 63 pp.

Guerlou-Demourgues, L., Denage, C., and Delmas, C. (1994) New manganese-substituted nickel hydroxides. Part 1. Crystal chemistry and physical characterization. *Journal of Power Sources,* **52,** 269–274.

Hachiya, K., Sasaki, M., Ikeda, T., Mikami, N., and Yasunaga, T. (1984) Static and kinetic studies of adsorption-desorption of metal ions on a γ-Al_2O_3 surface. 2. Kinetic study by means of pressure-jump technique. *Journal of Physical Chemistry,* **88,** 27–31.

Hansen, H.C.B., Kock, C.B., and Taylor, R.M. (1994) Synthesis and characterization of cobalt(II)-iron(III) hydroxide carbonate, a layered double hydroxide belonging to the pyroaurite group. *Journal of Solid State Chemistry,* **113,** 46–53.

Hemingway, B.S. and Sposito, G. (1996) Inorganic aluminum-bearing solid phases. In *The Environmental Chemistry of Aluminum,* G. Sposito, ed., CRC Lewis, Boca Raton, 81–116.

Lotmar, W. and Feitknecht, W. (1936) Uber anderungen der ionenabstande in hydroxyd-schichtengittern. *Zeitschrift für Kristallographie,* **A93,** 368–378.

Miyata, S. (1983) Anion-exchange properties of hydrotalcite-like compounds. *Clays and Clay Minerals,* **31,** 305–311.

Myneni, S.C.B., Tokunaga, T.K., and Brown, G.E., Jr. (1997) Abiotic selenium redox transformations in the presence of Fe(II,III) oxides. *Science,* **278,** 1106–1109.

Naumov, G.B., Ryzhenko, B.N., and Khodakovsky, I.L. (1974) *Handbook of Thermodynamic Data.* USGS, USGS-WRD-74-001, Menlo Park, 328 pp.

Navrotsky, A. (1994) *Physics and Chemistry of Earth Materials.* Cambridge University Press, Cambridge, 417 pp.

Nordstrom, D.K. and May, H.M. (1996) Aqueous equilibrium data for mononuclear aluminum species. In *The Environmental Chemistry of Aluminum,* G. Sposito, ed., CRC Lewis, Boca Raton, 39–80.

Nordstrom, D.K. and Munoz, J.L. (1994) *Geochemical Thermodynamics.* Blackwell, Boston, 493 pp.

Papelis, C., Hayes, K.F., and Leckie, J.O. (1988) HYDRAQL: A program for the computation of chemical equilibrium composition of aqueous batch systems including surface-complexation modeling of ion adsorption at the oxide/solution interface. Stanford University, Technical Report #306, Stanford, 130 pp.

Refait, P. and Genin, J.-M.R. (1997) Mechanisms of oxidation of Ni(II)-Fe(II) hydroxides in chloride-containing aqueous media: Role of the pyroaurite-type Ni-Fe hydroxychlorides. *Clay Minerals,* **32,** 597–613.

Rehr, J.J., Mustre de Leon, J., Zabinsky, S.I., and Albers, R.C. (1991) Theoretical x-ray absorption fine structure standards. *Journal of the American Chemical Society,* **113,** 5135–5140.

Reichle, W.T. (1985) Catalytic reactions by thermally activated, synthetic, anionic-clay minerals. *Journal of Catalysis,* **94,** 547–557.

Rucklidge, J.C. and Zussman, J. (1965) The crystal structure of the serpentine mineral, lizardite $Mg_3Si_2O_5(OH)_4$. *Acta Crystallographica,* **19,** 381–389.

Scheidegger, A.M., Fendorf, M., and Sparks, D.L. (1996) Mechanisms of nickel sorption on pyrophyllite: Macro-

scopic and microscopic approaches. *Soil Science Society of America Journal*, **60,** 1763–1772.

Scheidegger, A.M., Lamble, G.M., and Sparks, D.L. (1997) Spectroscopic evidence for the formation of mixed-cation hydroxide phases upon metal sorption on clays and aluminum oxides. *Journal of Colloid and Interface Science*, **186,** 118–128.

Scheidegger, A.M., Strawn, D.G., Lamble, G.M., and Sparks, D.L. (1998) The kinetics of mixed Ni-Al hydroxide formation on clay and aluminum oxide minerals: A time-resolved XAFS study. *Geochimica et Cosmochimica Acta*, **62,** 2233–2245.

Schindler, P.W., Liechti, P., and Westall, J.C. (1987) Adsorption of copper, cadmium, and lead from aqueous solution to the kaolinite/water interface. *Netherlands Journal of Agricultural Science*, **35,** 219–230.

Schutz, A. and Biloen, P. (1987) Interlamellar chemistry of hydrotalcites. *Journal of Solid State Chemistry*, **68,** 360–368.

Shannon, R.D. and Prewitt, C.T. (1969) Effective ionic radii in oxides and fluorides. *Acta Crystallographica*, **B25,** 925–946.

Smith, R.M. and Martell, A.E. (1997) *NIST Critical Stability Constants of Metal Complexes Database*. NIST, Gaithersburg, Maryland.

Subramanian, V. (1973) Mechanisms of fixation of the trace metals manganese and nickel by ferric hydroxide. Ph.D. thesis, Northwestern University, Evanston, Illinois, 89 pp.

Taylor, R.M. (1984) The rapid formation of crystalline double hydroxy salts and other compounds by controlled hydrolysis. *Clay Minerals*, **19,** 591–603.

Thompson, H.A. (1998) Dynamic ion partitioning among dissolved, adsorbed, and precipitated phases in aging cobalt(II)/kaolinite/water systems. Ph.D. thesis, Stanford University, Stanford, California, 117 pp.

Thompson, H.A., Brown, G.E., Jr., and Parks, G.A. (1997) XAFS spectroscopic study of uranyl coordination in solids and aqueous solution. *American Mineralogist*, **82,** 483–496.

Thompson, H.A., Parks, G.A., and Brown, G.E., Jr. (1999) Dynamic interactions of dissolution, surface adsorption, and precipitation in an aging cobalt(II)-clay-water system. *Geochimica et Cosmochimica Acta*, in press.

Towle, S.N., Bargar, J.R., Brown, G.E., Jr., and Parks, G.A. (1997) Surface precipitation of Co(II)(aq) on Al_2O_3. *Journal of Colloid and Interface Science*, **187,** 62–82.

Vucelic, M., Jones, W., and Moggridge, G.D. (1997) Cation ordering in synthetic layered double hydroxides. *Clays and Clay Minerals*, **45,** 803–813.

Yun, S.K. and Pinnavaia, T.J. (1995) Water content and particle texture of synthetic hydrotalcite-like layered double hydroxides. *Chemistry of Materials*, **7,** 348–354.

Zachara, J.M., Cowan, C.E., and Resch, C.T. (1991) Sorption of divalent metals on calcite. *Geochimica et Cosmochimica Acta*, **55,** 1549–1562.

(Received 11 August 1998; accepted 10 December 1998; Ms. 98-106)